

Soft cells and the geometry of seashells

Gábor Domokos  ^{a,b,*}, Alain Goriely  ^c, Ákos G. Horváth  ^{b,d} and Krisztina Regős  ^{a,b}

^aDepartment of Morphology and Geometric Modeling, Budapest University of Technology and Economics, Budapest, 1111, Hungary

^bHUN-REN-BME Morphodynamics Research Group, Budapest University of Technology and Economics, Budapest, 1111, Hungary

^cMathematical Institute, University of Oxford, Oxford, OX2 6GG, United Kingdom

^dDepartment of Algebra and Geometry, Budapest University of Technology and Economics, Budapest, 1111, Hungary

*To whom correspondence should be addressed: Email: domokos@iit.bme.hu

Edited By Michael Harris

Abstract

A central problem of geometry is the tiling of space with simple structures. The classical solutions, such as triangles, squares, and hexagons in the plane and cubes and other polyhedra in three-dimensional space are built with sharp corners and flat faces. However, many tilings in Nature are characterized by shapes with curved edges, nonflat faces, and few, if any, sharp corners. An important question is then to relate prototypical sharp tilings to softer natural shapes. Here, we solve this problem by introducing a new class of shapes, the soft cells, minimizing the number of sharp corners and filling space as soft tilings. We prove that an infinite class of polyhedral tilings can be smoothly deformed into soft tilings and we construct the soft versions of all Dirichlet–Voronoi cells associated with point lattices in two and three dimensions. Remarkably, these ideal soft shapes, born out of geometry, are found abundantly in nature, from cells to shells.

Keywords: tessellation, Nautilus shell, Dirichlet–Voronoi cell, tip growth

Significance Statement

Polygonal and polyhedral tessellations, consisting of cells with flat faces and sharp corners are successful models in geology, physics, and chemistry, describing phenomena ranging from crack networks to convection cells, foams and supramolecular patterns. However, these models fail to address the diversity of highly curved geometric shapes in biology. Here, we introduce a new class of tessellations, called soft tilings where cells have highly curved faces and the number of sharp corners is minimal, imitating constraints in biological growth. We prove a theorem demonstrating that soft tilings are abundant in the combinatorial sense and we demonstrate that these geometric shapes are strikingly reflected in natural examples, ranging from biological cells to the chambers of seashells, including the Nautilus.

Introduction

The quest to find tilings, i.e. space-filling patterns consisting of nonoverlapping, finite domains, started more than 10,000 years ago with the advent of masonry walls. However, tilings are much older than that: they are an integral part of Nature. Here, we describe a new class of space-filling patterns called soft tilings with highly curved cells which minimize the number of sharp corners. To motivate this concept, we first briefly review simpler tilings.

From Plato to Plateau: cells with flat and slightly curved faces

The first geometric theory of tilings dates back to Plato (1) who claimed that the five regular polyhedra, the Platonic solids, fill space without gaps, forming the four fundamental substances: earth, air, fire, and water, while the fifth solid (the dodecahedron) is

the building block of the cosmos. Plato's views were soon found to be flawed. Indeed, Aristotle claimed that only the cube and the tetrahedron can fill space without gaps. The latter statement is incorrect for the regular tetrahedron. However, there exist space-filling tetrahedral honeycombs (1) to which we will return later. Plato's idea was resurrected in the study of non-Euclidean honeycombs (2) where all Platonic solids fill space.

Plato's idea and Aristotle's refinement lead, ultimately, to the fundamental concept of the solid angle which proved to be an essential tool in describing the combinatorial properties of convex tilings (3, 4) which are also polyhedral tilings, filling space by convex polyhedra, without gaps and overlaps.

Polyhedral tilings provide good models for phenomena ranging from fragmentation processes (5) and the emergence of aeolian ridges on Mars (6) to supramolecular patterns in monolayers (7). However, in many cases the geometry of the natural tessellation appears to be more complex than a polyhedral tiling. Yet, these

Competing Interest: The authors declare no competing interest.

Received: April 18, 2024. **Accepted:** July 9, 2024

© The Author(s) 2024. Published by Oxford University Press on behalf of National Academy of Sciences. This is an Open Access article distributed under the terms of the Creative Commons Attribution-NonCommercial License (<https://creativecommons.org/licenses/by-nc/4.0/>), which permits non-commercial re-use, distribution, and reproduction in any medium, provided the original work is properly cited. For commercial re-use, please contact reprints@oup.com for reprints and translation rights for reprints. All other permissions can be obtained through our RightsLink service via the Permissions link on the article page on our site—for further information please contact journals.permissions@oup.com.



more intricate structures can still often be related to polyhedral tilings via *combinatorial equivalence*, which is a central concept in our work. If we imagine a tiling being constructed from rubber then, under elastic deformations, the shape of faces and edges can be largely distorted. However, if we require that material parts neither break apart nor are glued together in this process, then adjacent faces, adjacent edges, and adjacent nodes will remain adjacent, disjoint faces, disjoint edges, and disjoint nodes will remain disjoint. In this case, we call the original and the distorted tiling combinatorially equivalent (for a formal and more general definition, see Ref. (8)). Combinatorial equivalence is a fundamental tool in relating tilings with apparently different geometric features and finding such connections is one of the main goals of this study. In particular, in a tiling which is combinatorially equivalent to a polyhedral tiling, faces may not be planar and edges may not be straight. These properties are well reflected in the geometry of foams, controlled by Plateau's Laws: the Kelvin structure (9) and its improved version, the Weaire–Phelan structure (10), shown in Fig. 1. The small deviation in curvature observed in foams is the result of physical constraints, not the space-filling constraint. This idea was taken one step further in the description of the closely packed cell system of epithelia tissue (11). This geometric model, shown in Fig. 1b3, also has cells with curved faces and edges. While these cells are still individually combinatorially equivalent to polyhedra, the tiling as a whole is not combinatorially equivalent to any polyhedral tiling, showing that in this case curvature is a result of the constraint to fill space.

Despite having different reasons for being curved, all three aforementioned structures only differ slightly from polyhedral tilings in the sense that edges and faces meet transversely (angles both between faces and between edges are nonzero) and curvature radii along edges are very large compared to the size of the cell. This small deviation from polyhedral tilings may be the reason why such tilings are accepted as suitable models. Strikingly, in the theory of tilings no new category has been created to capture

phenomena where the curvature of cells and edges may be large enough to play a central role.

Large curvatures and the intuitive concept of soft tilings

If we keep the combinatorial structure of faces and vertices but we allow tangencies (zero angles) between them and we also allow faces and edges where curvature radii are comparable to the cell size, we enter an entirely new domain where radically new geometric features emerge. In particular, space-filling cells with tangencies and/or large curvatures may have fewer corners than polyhedral simplices and such cells (which, depending on the number of corners we will call either softened or soft) do emerge in Nature. Figure 2 illustrates 2D examples of cells with curved boundaries which have only two corners and 3D examples will be discussed in the next section.

To create a geometric framework for this generalization of polyhedral tilings, we introduce the concept of *polyhedral tilings* which includes, beyond polyhedral tilings, tilings with cells having zero internal angles, cells having strongly curved faces and/or edges; a formal definition is given in [Section S1A](#). We do not consider here pathological tilings by assuming for the rest of the article that both polyhedral and polyhedral tilings are *normal* and *balanced*, i.e. the cell diameter has uniform upper and lower bounds and the averages of cell and nodal degrees exist (4).

If a tiling consists of identical cells, we refer to the cells and to the tiling as *monomorphic*. In particular, if those cells are polyhedra then the tiling is *monohedral* and its curved generalization is called *monochedric*. There are infinitely many monohederal and monochedric tilings. Examples of monohederal tilings include the cubic grid and tilings with tetrahedral cells (1). An example of a monochedric tiling is the Kelvin structure of Fig. 1b1.

While the combinatorial properties of tilings have been investigated in detail, less attention was paid to the smoothness of the

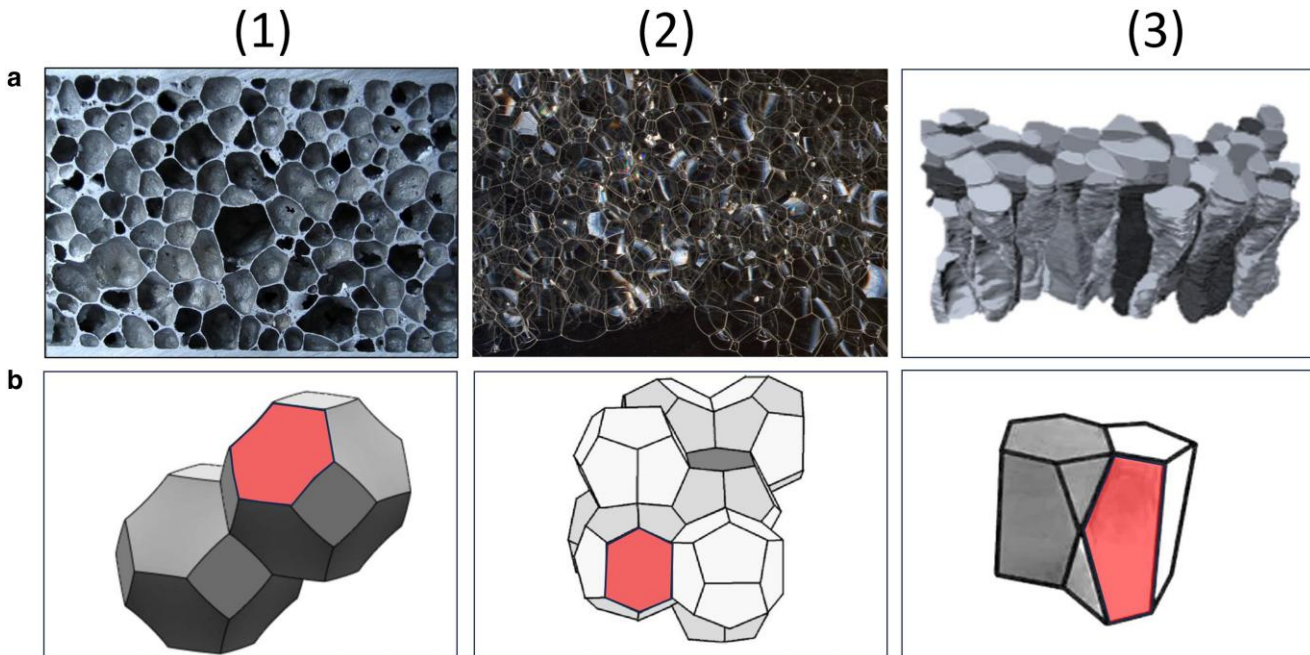


Fig. 1. Examples for slightly curved polyhedral tilings. Upper row: natural examples. Lower row: geometric models. One slightly curved face highlighted on each tiling. (a1) Metal foam (source: Wikimedia Commons) (a2) Liquid foam (source: Wikimedia Commons). (a3) Epithelia tissue (11). (b1) The Kelvin structure: a monohederal tiling. (b2) The Weaire–Phelan structure: a polyhederal tiling with two cells. Source (12, 13). (b3) Tiling with scutoids (14).

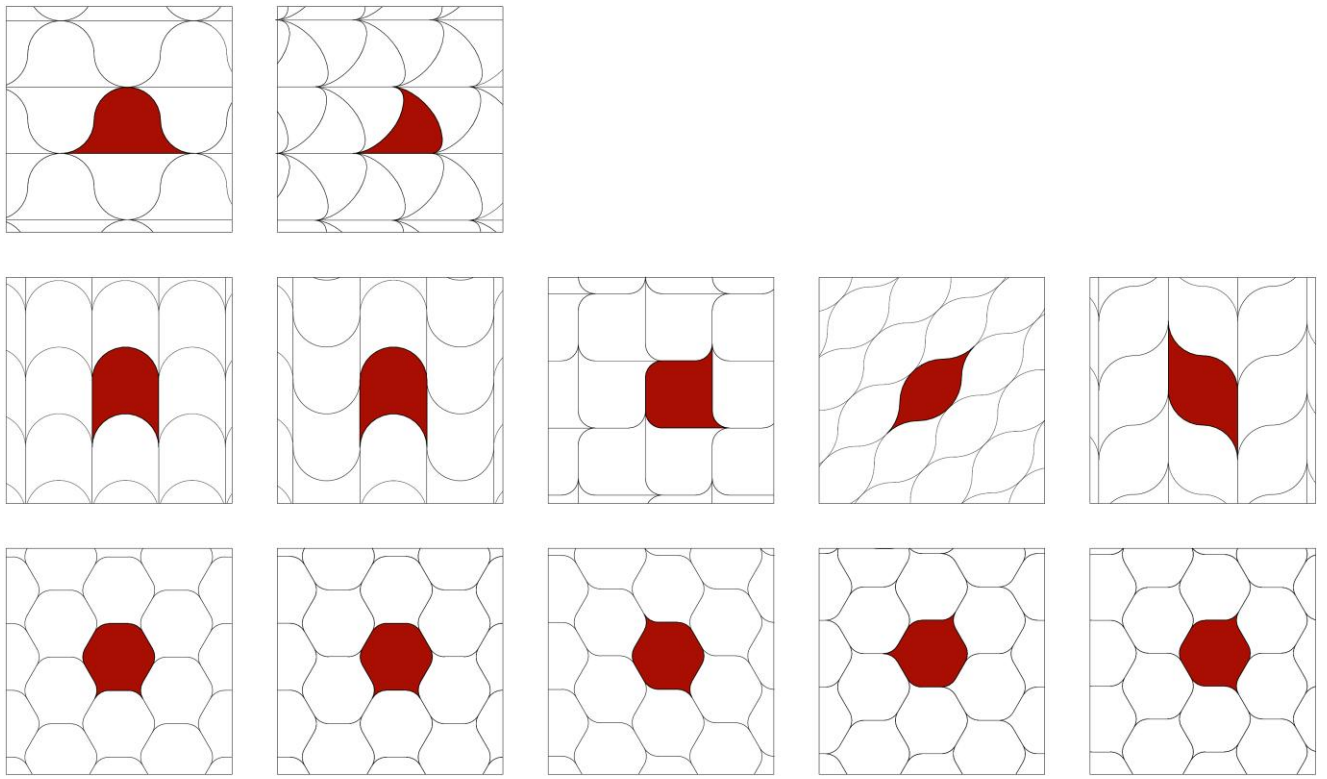


Fig. 2. Soft tilings in the plane. We show soft monohedric tilings which are combinatorially equivalent to monohedral tilings with regular polygons. Each row shows combinatorially equivalent soft tilings, corresponding to regular triangulation (first row), the rectangular grid (second row), and the hexagonal honeycomb (third row). If, beyond combinatorial equivalence classes, we also distinguish between sharp and soft corners then we arrive at the 12 tilings shown in the figure. We remark that the last two rows show soft tilings which are combinatorially equivalent to Dirichlet–Voronoi mosaics on point lattices (16).

cells. In 2D, shapes with at least C^1 -smoothness do not fill space (15). Since the planar sections of 3D tilings are 2D tilings and the generic planar sections of C^1 -smooth 3D objects are C^1 -smooth 2D objects, this property of 2D tilings also implies that a 3D tiling cannot consist entirely of C^1 -smooth tiles.

Since piecewise smooth shapes, such as squares and cubes, do fill space, and smooth shapes do not, a natural question is *how smooth* space-filling shapes can be. The answer to this question depends on how we measure smoothness. Using the concept of polyhedric tilings, we can assign a smoothness-related measure to monohedric cells and try to minimize this measure among possible space-filling shapes. Since a monohedric cell cannot be smooth, there exists a set of nonsmooth points on its boundary. Just as the smoothness of a point has various degrees (by counting the number of existing derivatives), we can define levels of *nonsmoothness* by counting the codimension of smooth manifolds containing the point. The basic idea is to reduce the number of points with highest level of nonsmoothness.

More precisely, we call a boundary point p of a cell a *corner* of the cell if no smooth curve on the boundary contains p . We denote the number of corners of a cell by v^* and we define v_{\min}^* as the minimal number of corners that a cell of a monohedric tiling may have (15). Both the $d = 2$ dimensional Euclidean plane and the $d = 3$ dimensional Euclidean space have monohedral simplicial (triangular and tetrahedral, respectively) tilings (19) with $v^* = d + 1$. Therefore, for $d = 2, 3$ we have $v_{\min}^* \leq d + 1$ and we will show that, in fact, this inequality is strict. The quantity v_{\min}^* was defined using the concept of monohedric tilings, however, we can also apply the very same quantity to classify general polyhedric tilings and cells. In d dimensions, we will call cells with $v^* \leq v_{\min}^*$ corners *soft cells*

and cells with $v_{\min}^* < v^* < d + 1$ corners *softened cells*. Analogously, we call a tiling consisting entirely of softened (soft) cells a *softened tiling* (soft tiling), for more detail, see [Section S1A](#).

Soft tilings and soft cells

Soft tilings in two dimensions

In 2D, corners are equivalent to the vertices along the boundary and it is known that on the Euclidean plane $v_{\min}^* = 2$ (15). Hence, in 2D we do not have softened cells and softened tilings. Figure 2 shows the monohedric soft tilings which are combinatorially equivalent to monohedral tilings with regular polygons which also includes all Dirichlet–Voronoi tilings on point lattices in the plane (16). Minimizing the number of corners may be seen as a guiding principle along which natural tilings evolved. Indeed, soft planar tilings emerge not only in natural patterns such as smooth muscle cells, seashells compartment, and zebra stripes, they have been repeatedly used in the works of visionary architect Zaha Hadid (a.k.a. the “Queen of Curves”), who abandoned the rectangular grid and created futuristic designs with curved facades. Figure 3 shows some soft tilings in 2D, how they appear in nature and in the work of Hadid.

Soft tilings in three dimensions

Unlike the 2D case, in 3D Euclidean space one can build a monohedric cell without any corners (15). Therefore, the absolute minimum $v_{\min}^* = 0$ can be reached which leaves the range $0 < v^* < 4$ for softened (but not soft) cells and tilings unexplored. We now proceed to study both soft and softened tilings.

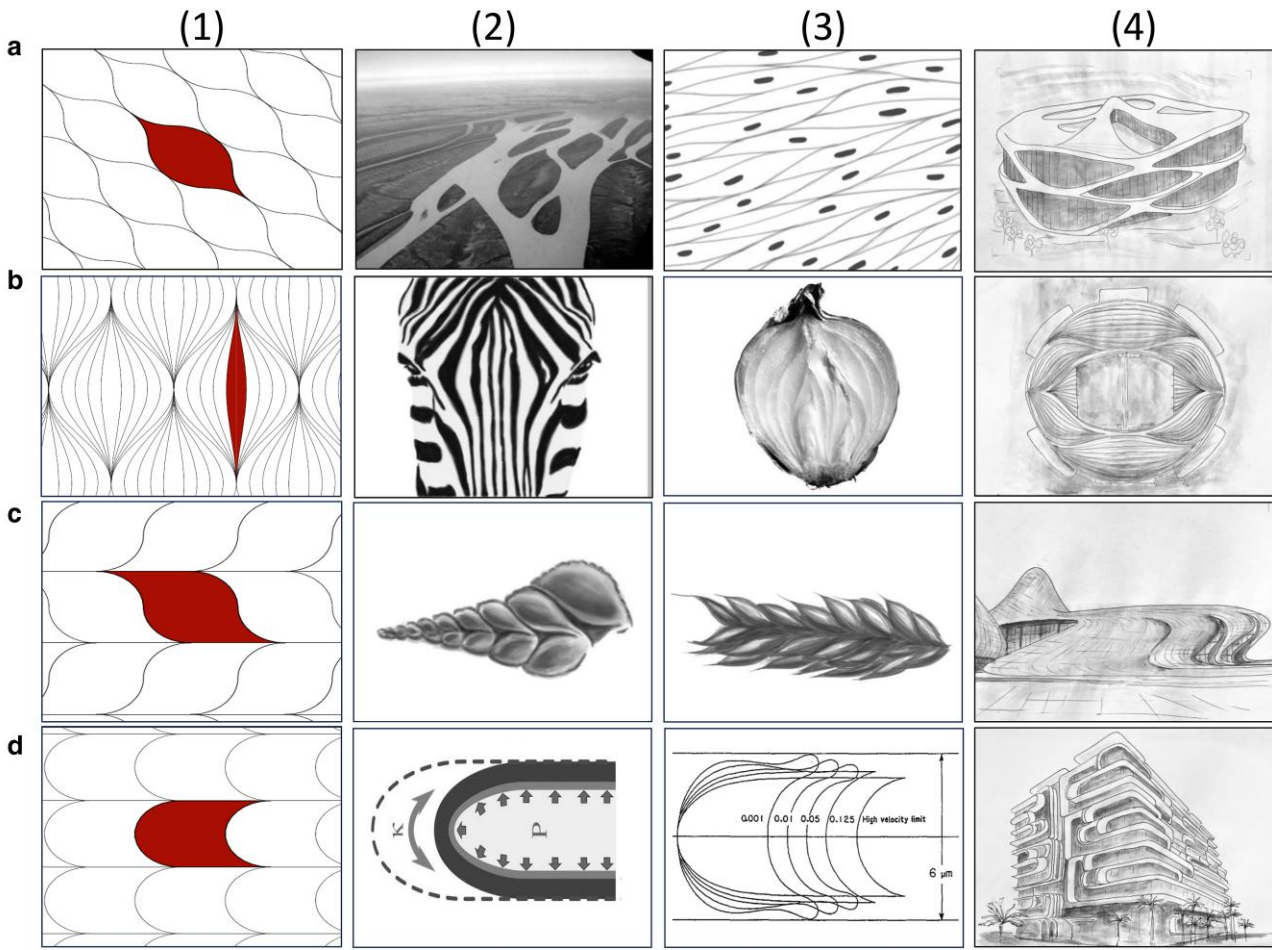


Fig. 3. Soft tilings in the plane: examples from nature and architecture. Column (1): examples of monohedric, soft tilings with $u^* = 2$ cells. (Remark that (a1), (c1), and (d1) are monohedric normal tilings, combinatorially equivalent to tilings with regular polygons, shown in Fig. 2, while (b1) is not a normal tiling.) Columns (2) and (3): examples in Nature where these patterns emerge. (a2) Betsiboka River estuary in northwestern Madagascar. Image credit: Wikimedia Commons. (b2) Zebra stripes. (c2) Cross section of see shell. (d2) Geometric model of tip growth in algae (17) (a3) Smooth muscle tissue. (b3) Cross-section of onion. (c3) Wheat awn (d3) meridian section of blood cell (18). Column (4): works of architect Zaha Hadid. (a4) Galaxy Soho, Beijing. (b4) Football stadium, Quatar. (c4) Heydar Aliyev Center, Baku (d4) Design for condominium in Surfside, Florida (2023). Image credit for (a3),(a4),(b2),(b3),(b4), c(2),c(3),c(4),d(4): Krisztina Regős.

As a stepping stone towards general soft 3D cells, and also serving as a link to applications in the geometry of seashells, we first define the concept of z-cells. A prism is generated by a simple, closed, piecewise smooth curve b_0 in the plane P and the family of all lines orthogonal to P and intersecting b_0 . We will refer to b_0 as the base of the prism and we will call planar sections orthogonal to P meridian sections. We call a compact shape a z-cell if its copies fill a prism without gaps and without overlaps (see Materials and methods, Construction of z-cells section, and [Section S3A](#).) We can distinguish between four types of z-cells, based on two binary properties: if the base of the prism is a monohedric tile in the plane then the z-cell is space-filling (otherwise it is not space-filling). If the cell has no sharp vertices, then it is soft (otherwise it is not soft). To the previous two, we add a third, independent binary category, applicable to any compact shape, determining whether or not it is a z-cell. These three binary properties generate the eight categories shown in Fig. 4 (see Materials and methods, Achieving high softness values section and [Sections S2B, S3, and S4A](#)).

The edge bending algorithm and the main theorem

Monohedric soft cells can be constructed from monohedral cells by the *edge bending algorithm*: We start with a polyhedral tiling

and smoothly bend each edge in such a manner that at each node all half-tangents are aligned. In this process, corners are converted into points of edges, i.e. into points at which all smooth curves of the boundary have identical tangents.

For example, consider the cubic grid, a space-filling polyhedral tiling consisting of cubes as cells, see Figs. 4c3 and 7b1. Three edges meet at any corner, their half-tangents pairwise at right angles (Fig. 7c1). As we apply the edge bending algorithm, we keep the vertical half-tangent frozen (see Fig. 7(1)) and bend the other two edges so their half-tangents become also vertical. In this manner all three half-tangents are aligned and the corner disappears (Fig. 7d1). Intuitively, one can achieve softened and soft tessellations by the edge bending algorithm, the details of which we discuss in Materials and Methods, subsection as well as in the [Section S1](#), and we illustrate the algorithm in [Supplementary Movie SM1](#).

The starting object for the edge bending algorithm is a convex (polyhedral) tiling and we will call the execution of the algorithm successful if it results in a soft tiling. Whether or not the edge bending process is successful for any arbitrary initial tiling is unknown. Edge bending is a complex geometric process transforming edges and faces while developing possibly large curvatures. Surprisingly, we show that a purely combinatorial condition on

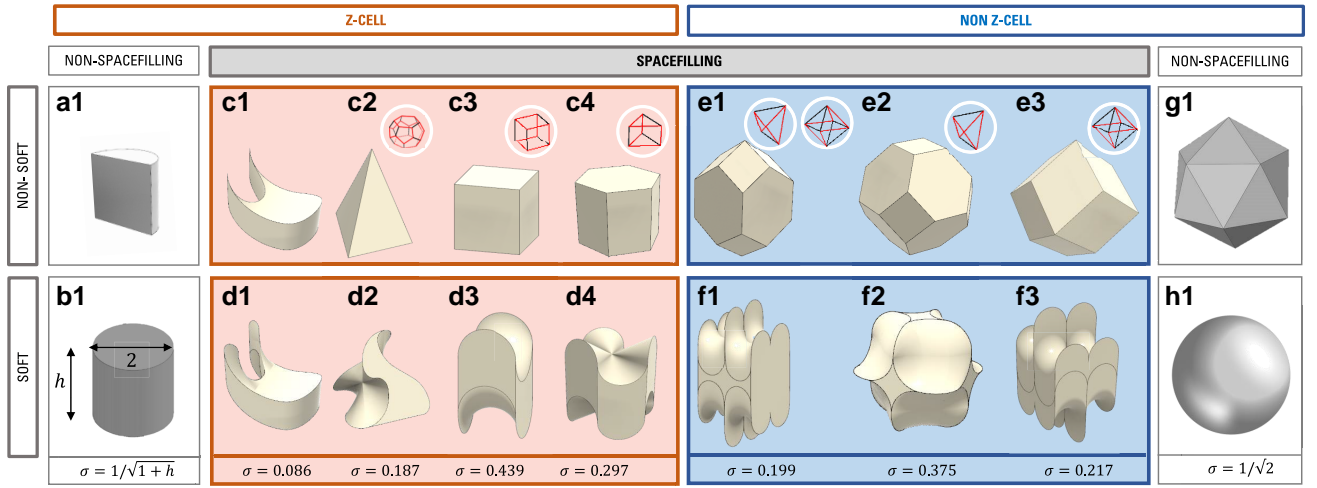


Fig. 4. Genesis of soft 3D cells. First row, a, c, e, g) nonsoft cells. Second row, b, d, f, h) soft cells, with softness value indicated below each cell. Insets in white circles show the dual of the vertex polyhedron with Hamiltonian circuit indicated in red. II. Individual panels: a1) Half cylinder: nonsoft, nonspacefilling cell. b1) Cylinder. Maximal softness ($\sigma = 1$) if $h = 0$ (two-sided circular disc). c1) Space-filling z-cell, resembling the Nautilus chamber. c2–c4) Monohedral cells of prismatic tilings. c2) Goldberg tetrahedron. c3, c4) Dirichlet–Voronoi lattice z-cells. c3) cube c4) hexagonal prism. d1–d4) Soft versions of c1–c4) as monohedric soft z-cells. e1–e3) Dirichlet–Voronoi lattice non-z cells. e1) Elongated dodecahedron. e2) Truncated octahedron. e3) Rombododecahedron. f1–f3) Soft versions of (c1–c3) as monohedric, soft, non-z-cells. g1) Nonspacefilling nonsoft cell: Icosahedron. h1) Nonspacefilling soft cell: sphere.

the initial tiling is sufficient for the algorithm to be successful. This condition hinges on three classic concepts which we briefly explain (see also [Supplementary Movie SM1](#)). Every polyhedron P is associated with a *dual polyhedron* P' in such a manner that the vertices of P correspond to the faces of P' and vice versa and the edges between pairs of vertices of P correspond to the edges between pairs of faces of P' and vice versa. For example, the dual of the cube is the octahedron and the tetrahedron is a self-dual polyhedron. If P is convex, so is P' . The second classic concept is a polyhedron's *Hamiltonian circuit*: a cyclic path along the edges of a polyhedron that visits each vertex exactly once. The condition for the nonexistence of a Hamiltonian circuit for a given polyhedron depends on the number of faces, edges and vertices. Necessary conditions (lower bounds) are known (20), but the exact minima for the number of faces, edges and vertices so that the polyhedron does not have a Hamiltonian circuit are not known, not even for simple polyhedra where three edges meet at every vertex. The third notion is the concept of a *vertex polyhedron*. The tiles of polyhedral tilings are polyhedra. The nodes of the tiling are points where the vertices of polyhedral cells overlap and the degree n_o of the node o is equal to the number of polyhedra the vertices of which overlap at o . If we consider the intersection of the tiling with a small sphere centered at o then we obtain a spherical polyhedron P_o with n_o faces. We call the Euclidean polyhedron (with straight edges and flat faces) which is combinatorially equivalent to P_o the *vertex polyhedron* at the node o . For example, in a regular cubic grid we have $n_o = 8$, vertex polyhedra are octahedra because 8 cubes meet at every node. Using these three key concepts, we give the necessary condition for the edge bending algorithm to be successful:

THEOREM 1: Let M be a balanced, normal convex tiling and let $\mathcal{V}(M)$ denote the set of the duals of vertex polyhedra in M . If every polyhedron $P \in \mathcal{V}(M)$ has a Hamiltonian circuit, then there exists a soft polyhedral tiling M' which is combinatorially equivalent to M .

As an example, consider the cubic grid with the octahedron as its vertex polyhedron. The dual of this vertex polyhedron is the

cube. Since there exists a Hamiltonian circuit on the cube (inset of Fig. 4c3), Theorem 1 guarantees that there exists a soft polyhedral tiling which is combinatorially equivalent to the cubic grid. The cell of one particular example, which happens to be monohedric, is shown in Fig. 4d3, and the corresponding tiling is shown in Fig. 7e1. We provide the proof of the Theorem in the [Section S1](#). Whether or not the sufficient condition in Theorem 1 is also necessary is not clear. However, we believe that this condition can be relaxed:

CONJECTURE 1: Let M be a balanced, normal, convex tiling. Then, there exists a combinatorially equivalent, soft polyhedral tiling M' .

Theorem 1 shows, in broad terms, that soft tilings are ubiquitous in the combinatorial sense. Indeed, Fig. 4c3, c4, e1, e2, and e3 shows all five Dirichlet–Voronoi cells of point lattices (16, 21) with insets of the duals of the vertex polyhedra. In every case, it is easy to build a Hamiltonian circuit. We remark that, beyond the Dirichlet–Voronoi tessellations of point lattices, the condition set in Theorem 1 also proves to be sufficient for all uniform honeycombs. In fact, we are not aware of any monohedral tiling where the dual of the vertex polyhedron does not have either a Hamiltonian path (if the edge graph is simple) or a Hamiltonian circuit.

Soft, softer, softest

The geometry of convex monohedral tilings is constrained: for example, the shape of the five Dirichlet–Voronoi cells of point lattices (16, 21), illustrated in Fig. 4c3, c4, e1, e2, and e3 is completely determined by the lattice. By using the edge bending algorithm introduced above, we constructed the corresponding soft monohedric tilings, the five soft cells of which are shown in Fig. 4d3, d4, f1, f2, f3. (For more details, see [Sections 2B and 4A](#).) While the shape of the Dirichlet–Voronoi polyhedral cells is exactly determined by the lattice, the exact shape of the corresponding soft cells is not uniquely defined.

To understand better the geometry of soft cells and to relate them to physical realizations, we introduce a continuous scale

on softness for 3D shapes. In the spirit of Blaschke's Rolling Ball Theorem (22), we imagine that two identical circular disks are rolled along the opposite sides of a planar curve c in such a manner that their contact point at $P_c \in c$ is always identical. We call the maximal radius of these disks under the condition that they can be both rolled smoothly locally at P_c the *rolling radius* of c at P_c and denote it by $\rho(P_c)$. If c is at least C^2 -smooth at P_c then $\rho(P_c)$ is identical to the radius of curvature of c at P_c but if c has a vertex at P_c , no finite disk can be smoothly rolled and we have $\rho(P_c) = 0$. We can generalize this concept to topological spheres S embedded into 3D space as follows. Let P_S be a point on the boundary of S . Then, the rolling radius $\rho(P_S)$ of S at P_S is defined as the supremum of the rolling radii of any planar section of S at P_S . We call the infimum of rolling radii of all points P_S on the boundary of S the rolling radius $\rho(S)$ of S . We define the softness of S as

$$\sigma(S) = \rho(S) \sqrt{\frac{2\pi}{A(S)}}, \quad (1)$$

where $A(S)$ is the surface area of S . If S is at least C^2 -smooth then $\rho(S)$ is the infimum of radii corresponding to the smaller principal curvature and $\rho(S) = 0$ as soon as S has a sharp corner. As an example consider the family S_a of oblate spheroids with semi-axes $(a, 1, 1)$ with $0 \leq a \leq 1$. Here, we have $\rho(S_a) = 1$ for every value of a (see Section S3), so $\sigma(S_a)$ only depends on the surface area which is a monotonic function of a as $\sigma(S_a) = \sqrt{e/(e + a \operatorname{artanh}(e))}$, where $e = \sqrt{1 - a^2}$ and $\operatorname{artanh}(e)$ is the inverse hyperbolic tangent of the eccentricity e . The sphere has $\sigma(S_1) = 1/\sqrt{2}$ and the circular disc has $\sigma(S_0) = 1$ (see Fig. 4b1) and the latter case seems to be the global supremum of softness for all compact bodies.

Using the above concept, we can now further deform a soft tiling to maximize its softness. We found rules (see Materials and methods, Achieving high softness values section) which resulted in relatively high softness values. We compute and give the softness for the cells in Fig. 4d1–d4, f1–f3 by using (1). It is not clear whether any of these cells have maximal softness but the soft monohedric cells in panels (d3, d4, f1, f2, f3) corresponding to the five Dirichlet–Voronoi cells on lattices appear to have softness close to the maximum if the lattice is fixed (see Section S4A for details on the computation). However, in case of (d3) and (d4), softness can be further increased by changing the lattice so that the distance between the two curved faces decreases.

Soft cells in nature

Establishing and maintaining sharp corners in physical cells is difficult and costly as surface tension and elasticity naturally tend to smooth corners. Hence, it is not surprising that many soft tilings are found in Nature. For instance, soft z-cells appear to be ideal models for a variety of natural shapes such as tip growth, one of the most ubiquitous biological shape evolution processes (23–25). Z-cells also describe well the shape of blood cells travelling through capillaries (18) (cf. Fig. 3d2 and d3). But, perhaps the most striking appearance of such structures is found in the chambers of some seashells that we now explore.

The soft geometry of chambered seashells

Chambered seashells are a fascinating feature found in certain mollusks, primarily in cephalopods. The most well-known examples include the extinct ammonites with shells divided into chambers connected by a tube, the *siphuncle*, and the extant nautilus, well known for its iconic spiral divided into chambers. The animal

lives in the outermost chamber and uses the siphuncle in order to control buoyancy by adjusting the gas-to-liquid ratio in the chambers. This is done by removing water from the chambers and replacing it with gas, which is mainly nitrogen, carbon dioxide, and argon in the case of the nautilus.

The chambers in segmented seashells grow under the constraint to fill the space provided by the outer shell. The geometry of the chambers has been investigated only recently, MicroCT technology providing unprecedented access to 3D images (26, 27) of which Fig. 4 shows two examples. The curved, soft contours of both chambers immediately catch the eye. The curved, spiral geometry of the tubular shell has no direct bearing on the softness of the chambers. Following Seilacher (28), we model the tubular shell as a prismatic object: the contour of the tube, orthogonal to the z axis is the base b_0 of the prism in the geometric model (see also Fig. 7(1)). Since the contour b_0 of shells tends to be smooth, if the tube is segmented in a generic fashion by a smooth interface M_1 and its parallel z -translation M_2 (serving as the geometric model of septa), then the intersection lines b_1, b_2 , defining a finite shell segment, are also smooth and the segments of the prism, modeling shell chambers emerge as soft z -cells (for a detailed discussion on the geometry of soft z -cells, see Materials and methods, Construction of z -cells section). Geometric models of shell chambers were developed by Seilacher in a series of seminal papers (28–30). Here, we discuss two of his models, the *paper model* and the *balloon model* describing the geometry of septal walls with vanishing and with positive Gaussian curvature, respectively. Despite the fact that these models are qualitative, they both predict that the respective shell chambers will be soft z -cells. Each model can approximate some aspects of the shell chamber's geometry, however, in some cases one of the models may offer a good approximation on its own and in Fig. 5 we examine such special shell chambers.

The first example is an extinct ammonite genus (*Cadoceras*). Relying on Micro CT datasets presented in (27) we traced the cross-section b_0 and the spatial contours b_1, b_2 , characterizing the shape of the chamber. All three contours are smooth, and septal walls can be closely approximated by a surface with vanishing Gaussian curvature. Therefore they define a soft, non-spacefilling z -cell (see Fig. 5a1–a4) the geometry of which is well approximated by Seilacher's paper model.

Our second example is the shell of an extant species, the deep water mollusk *Spirula spirula*. Here the septal walls resemble spherical caps with nonvanishing Gaussian curvature and they are well approximated by the balloon model. As before, the model of the chambers emerges as a soft, non-spacefilling z -cell (see Fig. 5b1–b4).

The chamber of the nautilus

The most famous example of chambered seashells is undoubtedly the nautilus (*Nautilus belauensis*) which has been subject of geometric interest (31, 32) ever since the seminal book (33) of D'Arcy Thompson appeared in 1917, pointing out that the 2D geometry of the section in the plane of symmetry is a good approximation of the logarithmic spiral. Here we show that the 3D geometry of the chamber is not only a good approximation of a soft z -cell (like other chambered shells), but it is also a good approximation of a soft, space-filling, monohedric cell. Indeed, Fig. 6(4) shows the striking visual resemblance between the nautilus chamber (26) and its soft, spacefilling geometric model.

The latter was created using two orthogonal sections of the shell, illustrated in Fig. 6a1 and we simplified these two sections

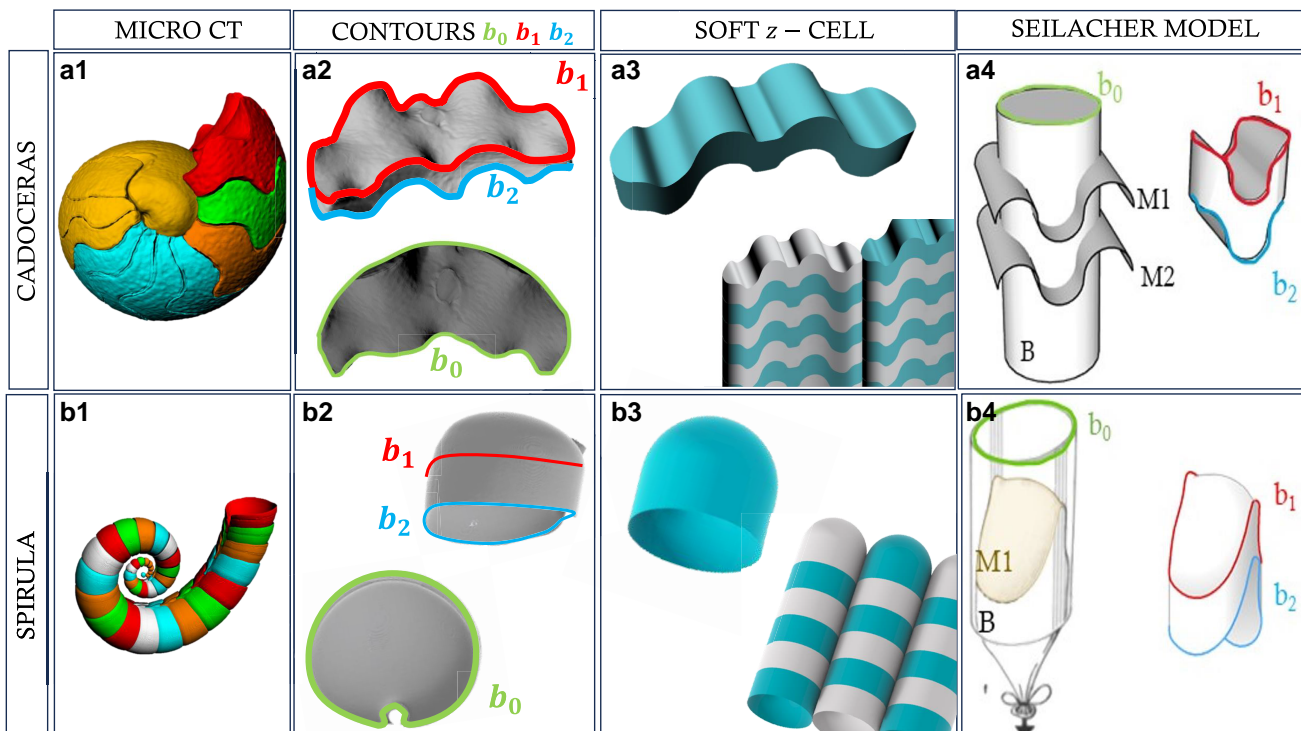


Fig. 5. Soft cells in chambered shells. Upper row: Ammonite shell chambers (*Cadoceras*) (a1) All chambers, reconstructed from micro CT dataset (27). (for details see [Supplementary Information](#)). a2) Individual chamber with smooth upper and lower contours b_1 , b_2 and base contour b_0 . a3) Soft, nonspacefilling z-cell as model of *Cadoceras* chamber. a4) Seilacher's paper model for septa: cylinder with base b_0 intersected by two smooth surfaces along curves b_1 , b_2 (29). Bottom row: the chamber of the extant *Spirula spirula* shell. b1) All chambers, reconstructed from micro CT dataset (27). b2) Individual chamber with smooth upper and lower contours b_1 , b_2 and base contour b_0 . b3) Soft, nonspacefilling z-cell as model of the *Spirula* chamber. b4) Seilacher's balloon model: inflated balloons glued along the curves b_1 , b_2 to the wall of cylinder with base b_0 (29).

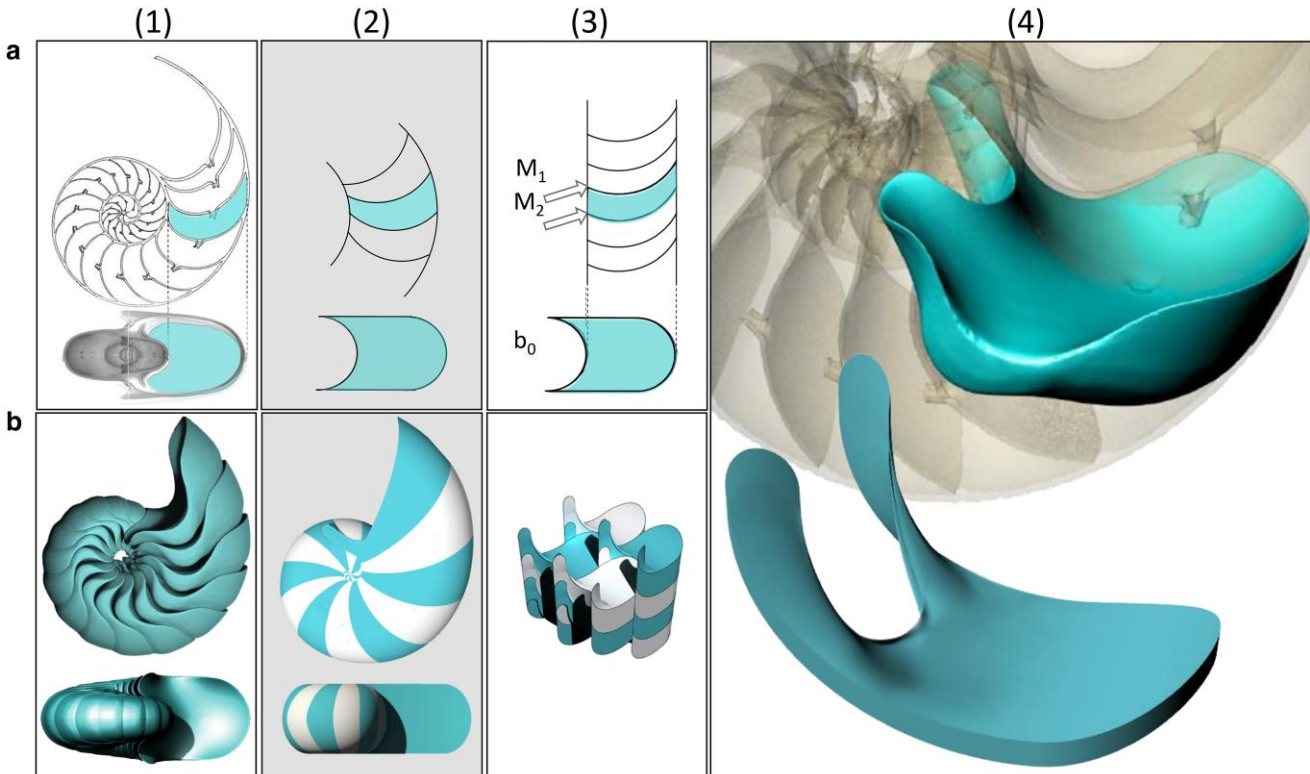


Fig. 6. The geometry of the nautilus chamber. Row (a): Sections. Row (b): 3D geometry. Column (1) Measured datasets, using data from (26). Column (2): Spiral model. Column (3): Prismatic model. Panel (4): Visual comparison between the nautilus chamber and its geometric model. For the geometric operations connecting (3a) to (3b) see Fig. 7, row (2).

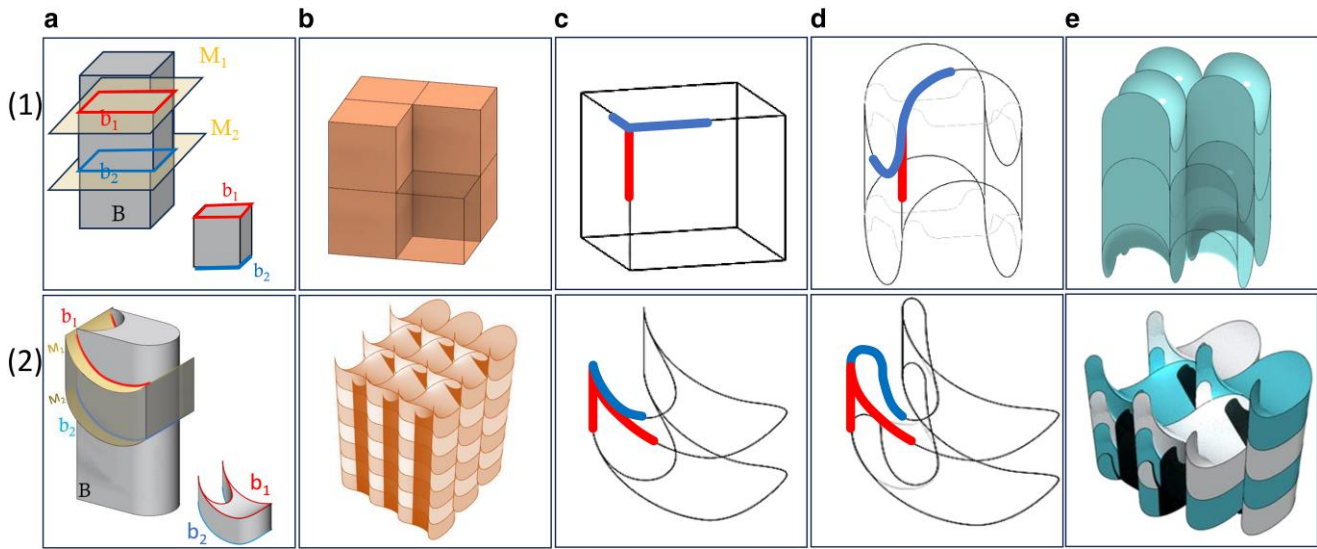


Fig. 7. Geometry of z-cells and the edge bending algorithm. Row (1): Cubic cell. Row (2): Nautilus cell. Columns: a) Genesis of z-cell: intersecting of prism B with manifolds M_1 , M_2 produces z-cell with respective lower and upper contours b_1 , b_2 . b) prismatic tiling by z-cells. c) Wireframe model of z-cell. Red line marks specified direction at node, blue lines mark edges not aligned with the red direction. d) Spacefilling z-cell transformed into soft, spacefilling z-cell by edge bending. Red edges did not change, blue edges have been bent. e) prismatic tiling by soft z-cells.

in two steps (see Fig. 6a2 and a3) to obtain a geometric model. In the first step, we assumed that the mostly flat shell is ideally flat, i.e. it is constrained between two parallel walls. We call this the *flatness assumption* and the resulting model the *spiral model*. In the second step, following Seilacher (30), we simplified the meridian section to be that of a straight prism and we call this the *prismatic assumption* and the resulting model the *prismatic model*. The flatness assumption results in a soft, monohedric planar cell (cf. Figs. 6a2 and 3d1) as the base b_0 of the prism in the prismatic assumption. We used the sections shown in Fig. 6a3 to create the 3D model of the chamber in two steps (see Materials and methods, Construction of z-cells section and Fig. 7). In the first step, the prism is intersected by two parallel, cylindrical surfaces resulting in a softened, space-filling z-cell with two sharp corners. In the second step, we use the edge bending algorithm to soften this cell, resulting in a space-filling, soft cell shown next to the chamber in Fig. 6(4). Figure 6b1 shows how the chambers fill the shell, Fig. 6b3 shows how the geometric model of the chamber fills 3D space, and Fig. 6b2 illustrates the geometry of the model without the prismatic assumption. As we can see, in the spiral model we also have a soft, space-filling tiling, albeit not a normal tiling: due to the spiral geometry the tiling includes both infinitely small and infinitely large cells. We also remark that, unlike the examples in Fig. 5, the shape of the nautilus chamber can only be captured by combining two different Seilacher models (see Section S5).

Summary and outlook

We introduced a new class of shapes called *soft cells* that tile 2D and 3D Euclidean space and have a minimal number of sharp corners. In 2D, this implies having $v^* = 2$ corners while in 3D soft cells have no sharp corners. The lack of sharp corners and their soft, highly curved geometry makes soft cells ideal candidate models for biological structures which evolved under full or partial constraint to fill space. An important special class, representing partial constraint, are soft z-cells which fill prismatic tubes without gaps. Similar constraints arise in biological growth, and we can

observe shapes strongly reminiscent of soft z-cells not only among blood cells traveling at high speed but also in tip growth and in the chambers of seashells. In particular, the Nautilus shell not only exhibits chambers with the geometry of soft z-cells but these cells are remarkably close to space-filling z-cells.

Soft cells are not only abundant in Nature: we gave a sufficient condition under which a polyhedral tiling can be continuously transformed into a soft tiling. In fact, the proof (given in Section S1C and D) shows that a broader claim is also true: even if the original tiling is not polyhedral, as long as the vertex polyhedron's dual has a Hamilton circuit, the edge bending algorithm can be executed and the tiling can be turned into a soft tiling. This encompasses a broad class of tessellations, including, for example, tessellations by scutoids (14).

Beyond Nature and mathematics, we also find soft cells emerging in art. In Fig. 3, we showed examples of 2D soft cells appearing in the work of Zaha Hadid. However, there are other notable artists, like Katsushika Hokusai or Victor Vasarely, who depict soft 2D cells (see Section S4B). Even 3D soft cell seem to have roots in art, albeit in a curious manner. It not only appears that architects used such shapes to avoid corners, they even claimed to have identified the soft cell in Fig. 4d3 by a construction starting from the Gömböc shape (34). In the Section S4B, we show this design along with another building which reflects the shape of the soft 3D cell in Fig. 4d4.

Open questions

This new class of shapes suggests several questions, the answers to which could shed more light on their geometry and the connections to nature. From a mathematical point of view, a proof of Conjecture 1 would be most desirable. However, there are other interesting questions related to the edge bending algorithm. While the latter always preserves the combinatorial structure of the tiling, metric properties may or may not be preserved. Most notably, the number of congruence classes for the tiles may change and if the initial tiling was monohedric, it may not be possible to produce a monohedric soft tiling by this algorithm. Since we were particularly interested in soft monohedric tilings, the

examples in this article illustrated cases where the algorithm preserved the monohedric property of the tiling. This is always possible, as long as we have a lattice-like tiling with a single cell as fundamental domain. This condition is certainly not necessary, the tetrahedral soft cell in Fig. 4d2 is part of a monohedric tiling which is not lattice-like (full tiling shown in Section S4, Fig. S17). Any necessary condition appears to be nontrivial, since there are many monohedral tilings, the soft version of which is not monohedric. The simplest such example is probably a planar triangulation, created by a rectangular grid with all diagonals added. Other examples can be found among monohedral pentagon tilings (35) and one most notable example is the recently discovered aperiodic monotile (“einstein”) (36) and its chiral version (37). Both have 13 sharp corners the number of which cannot be reduced if we want to preserve the monohedric property of the tiling. Hence, we pose the question what is minimal number of sharp corners for an aperiodic monotile.

From the point of view of applications, we showed examples where 2D soft cells helped to describe natural patterns, and we found several natural phenomena where 3D soft z-cells appear to describe the essence of the geometry. Still, we have not yet found any example of a soft, 3D non-z-cell appearing in Nature, although, as Fig. 4 illustrates, these attractive shapes appear to be abundant in geometry. We believe that finding an example of a soft non-z cell in Nature would greatly help to understand the connection between growth processes and this new class of shapes.

Materials and methods

Construction of z-cells

As stated in the main text, z-cells are constructed by the segmentation of infinite prisms with axis z into identical, finite parts. Here, we only consider the case where adjacent z-cells are related by z-translation. (For the general case, see Section S3A.) Figure 7 shows two such examples: the cubic cell (upper row) and the geometric nautilus cell (bottom row), both also shown in Fig. 4c1, d1, c3, and d3, respectively. We consider a smooth manifold M_1 which intersects the prism B with base b_0 in such a manner that it has exactly one transverse intersection point with every straight line on the boundary of B and we call the curve consisting of these points b_1 . The manifold M_2 is a z-translation of M_1 and intersects B in the curve b_2 which is the z-translation of b_1 . The curves b_1, b_2 define a finite segment \mathcal{B} of the prism B, and we call this segment a z-cell. If both the base b_0 of the prism and the manifold M_1 are smooth then b_1, b_2 are also smooth and \mathcal{B} will be a soft z-cell.

Edge bending

In the edge bending algorithm (see also [Supplementary Movie SM1](#)), we consider a nonsoft space-filling cell with sharp corners as initial condition. At each sharp corner, we specify one straight line and bend all edges in such a manner that, on one hand, their half-tangents become aligned with the specified line, on the other hand, there is at least one half tangent associated with both directions defined by the line. Most conveniently, the specified line coincides with one of the half-tangents. While several edges become curved in this process, the combinatorial structure of the cell is not changed. To maintain the space-filling property of the cell, we have to pick the same straight line for every sharp vertex meeting at any node. In the case of the cubic cell (Fig. 7, upper row), it implies that we have to pick parallel lines at every vertex of the cell since all vertices meet at one node.

Achieving high softness values

To achieve high softness in the edge bending process, we always specify two co-planar lines e and f at sharp corners connected by an edge. Subsequently, we replace the edge by a Dubins path (38) under the constraint that the fixed curvature should be minimal. The lines e and f define four infinite planar domains in the generic case and three domains if they are parallel and the original straight edge is contained in exactly one of those domains. We construct the Dubins path under the additional constraint that it should also be contained in the same planar domain as the original edge. After tracing the edges by this algorithm, we select the set of (possibly curved) edges which correspond to the boundary of a face and construct a minimal surface on each face. The soft cells in Fig. 4d2-d4 and f1-f3 have been constructed by this algorithm. Whether or not they have maximal softness is not clear, with the possible exception of d3 and d4.

Acknowledgments

The authors thank Lajos Czeglédi for his invaluable help with 3D data rendering and presentation. It is also our great pleasure to thank Rene Hoffmann (Ruhr-Universität Bochum) and Robert Evan Lemanis (TU Dresden) for giving us access to their data on ammonite shells.

Supplementary Material

[Supplementary material](#) is available at PNAS Nexus online.

Funding

This research was supported by NKFIH grants K134199 and EMMI FIKP grant VIZ to K.R. and G.D. This research has been supported by the program EKÖP-24-3 funded by ITM and NKFI to K.R. The research was also supported by the Doctoral Excellence Fellowship Programme (DCEP) funded by ITM and NKFI and the Budapest University of Technology and Economics. The gift representing the Albrecht Science Fellowship is gratefully appreciated. This work was made possible through an International Exchanges Scheme Award from the Royal Society to A.G.

Author Contributions

G.D. designed research, all authors performed research; K.R. and G.D. analyzed data; A.G. provided context in biology; all authors wrote the article; A.G.H., K.R., and G.D. proved Theorem 1; K.R. and G.D. did 3D design.

Preprint

A preprint of this article is published at <https://arxiv.org/abs/2402.04190>.

Data Availability

The data for the Nautilus shell is the microCT scan performed by C. Erolin at the University of Dundee Museum Collections, available at <https://sketchfab.com/3d-models/nautilus-shell-sectioned-7c9e391fdbd5043e6bc1a044b9fb76905>. The data for the Ammonite shells are from Rene Hoffmann (Ruhr-Universität Bochum) and Robert Evan Lemanis (TU Dresden) and is available from them, at request.

References

- 1 Senechal M. 1951. Which tetrahedra fill space? *Math Mag.* 54(5): 227–243.
- 2 Coxeter HSM. 1956. Regular Honeycombs in hyperbolic space. In: Proceedings of the international congress of mathematicians, 1954. Vol. 3. pp 155–169, North-Holland, Amsterdam.
- 3 Schattschneider D, Senechal M. 2004. Tilings. In: Discrete and computational geometry. NW Boca Raton: CRC Press.
- 4 Schneider R, Weil W. 2008. Stochastic and integral geometry. Berlin, Heidelberg: Springer Science & Business Media.
- 5 Domokos G, Jerolmack DJ, Kun F, Török J. 2020. Plato's cube and the natural geometry of fragmentation. *Proc Natl Acad Sci U S A.* 117(31):18178–18185.
- 6 Nagle-McNaughton TP, Scuderi LA. 2021. Networked configurations as an emergent property of transverse aeolian ridges on Mars. *Commun Earth Environ.* 2(1):217.
- 7 Regős K, et al. 2023. Polygonal tessellations as predictive models of molecular monolayers. *Proc Natl Acad Sci U S A.* 120(16): e2300049120.
- 8 Grünbaum B, Shepard GC. 1987. Tilings and patterns. New York: Freeman and Co.
- 9 Weaire D. 2009. Kelvin's ideal foam structure. *J Phys Conf Ser.* 158: 012005.
- 10 Weaire D, Phelan R. 1994. The structure of monodisperse foam. *Philos Mag Lett.* 70(5):345–350.
- 11 Gómez HF, Dumond MS, Hodel L, Vetter R, Iber D. 2021. 3d cell neighbour dynamics in growing pseudostratified epithelia. *eLife.* 10:e68135.
- 12 Bitsche R. 2005. Space-filling polyhedra as mechanical models for solidified dry foams [master's thesis]. Technical University of Vienna.
- 13 Daxner T, Bitsche RD, Böhm HJ. 2006. Space-filling polyhedra as mechanical models for solidified dry foams. *Mater Trans.* 47(9): 2213–2218.
- 14 Gómez-Gálvez P, et al. 2018. Scutoids are a geometrical solution to three-dimensional packing of epithelia. *Nat Commun.* 9(1): 2960.
- 15 Domokos G, Horváth AG, Regős K. 2023. A two-vertex theorem for normal tilings. *Aequationes Math.* 97(1):185–197.
- 16 Horváth ÁG. 1996. On the Dirichlet–Voronoi cell of unimodular lattices. *Geom Dedicata.* 63:183–191.
- 17 Rabillé H, et al. 2019. The brown algal mode of tip growth: keeping stress under control. *PLoS Biol.* 17(1):e2005258.
- 18 Secomb TW. 1991. Red blood cell mechanics and capillary blood rheology. *Cell Biophysics.* 18(3):231–251.
- 19 Goldberg M. 1974. Three infinite family of tetrahedral space-fillers. *J Comb Theory (A).* 16(3):348–354.
- 20 Barnette D, Jucovi E. 1970. Hamiltonian circuits on 3-polytopes. *J Comb Theory.* 9(1):54–59.
- 21 Voronoi GF. 1909. Nouvelles applications des paramètres continus à la théorie des formes quadratiques ii. *Geom Dedicata.* 136:67–181.
- 22 Brooks JN, Strantzen JB. 1989. Blaschke's rolling ball theorem in R^n . Providence, Rhode Island, USA: Memoirs of the AMS. No. 405. ISSN 0065-926680.
- 23 Goriely A. 2017. *The mathematics and mechanics of biological growth.* New York: Springer Science and Business Media.
- 24 Goriely A, Tabor M. 2008. Mathematical modeling of hyphal tip growth. *Fungal Biol Rev.* 22(2):77–83.
- 25 Reinhhardt MO. 1892. Das wachsthum der pilzhphen. (No Title).
- 26 Erolin C. 2017. [dataset] nautilus shell (sectioned), micro ct 3d model. University of Dundee Museum Collections, <https://sketchfab.com/3d-models/nautilus-shell-sectioned-7c9e391fb5043e6bc1a044b9fb76905>
- 27 Lemanis R, Korn D, Zachow S, Rybacki E, Hoffmann R. 2016. The evolution and development of cephalopod chambers and their shape. *PLoS One.* 11(3):e0151404.
- 28 Seilacher A. 1973. Fabricational noise in adaptive morphology. *Syst Zool.* 22:451–465.
- 29 Seilacher A. 1975. Mechanische simulation und funktionelle evolution des Ammoniten-Septums. *Paläont Z.* 49:268–286.
- 30 Seilacher A, Labarbera M. 1995. Ammonites as Cartesian divers. *PALAIOS.* 10(6):493–506.
- 31 Hewitt RA, Westermann GEG. 2010. Nautilus Shell Architecture. In: Saunders WB, Landman NH editors. Nautilus. Topics in Geobiology. Vol 6. Dordrecht: Springer.
- 32 Moulton DE, Goriely A, Chirat R. 2015. The morpho-mechanical basis of ammonite form. *J Theor Biol.* 364:220–230.
- 33 Thompson DW. 1917. *On growth and form.* Cambridge, UK: Cambridge University Press. (second edition 1942, and abridged editions by Bonner, J. T., 1961 & 1992).
- 34 Santos S. 2015. The whole building's a stage in this conceptual cirque du soleil theatre design. ArchDaily, <https://www.archdaily.com/769620/the-whole-buildings-a-stage-in-this-conceptual-cirque-du-soleil-theatre-design>:July 5th.
- 35 Mann C, McLoud-Mann J, Von Derau D. 2018. Convex pentagons that admit i-block transitive tilings. *Geom Dedicata.* 194(1):141–167.
- 36 Smith D, Myers JS, Kaplan CS, Goodman-Strauss C. 2024. An aperiodic monotile. *Combinatorial Theory.* 4(1). <http://dx.doi.org/10.5070/C64163843>
- 37 Smith D, Myers JS, Kaplan CS, Goodman-Strauss C. 2023. A chiral aperiodic monotile, arXiv, arXiv:2305.17743, preprint: not peer reviewed. <https://doi.org/10.48550/arXiv.2305.17743>
- 38 Dubins LE. 1957. On curves of minimal length with a constraint on average curvature, and with prescribed initial and terminal positions and tangents. *Am J Math.* 79(3):497–516.